34th Annual International Conference of the IEEE EMBS
San Diego, California USA, 28 August - 1 September, 2012

Foam Phantom Development for Artificial Vertebrae used for Surgical Training

David Fuerst[1,3], Daniel Stephan[2,3], Peter Augat[2,3] and Andreas Schrempf[1]

***Abstract*—Currently the surgical training of kyphoplasty and vertebroplasty is performed on patients or specimens. To improve patient safety, a project was initiated to develop an Augmented Reality simulator for the surgical training of these interventions. Artificial vertebral segments should be integrated to provide realistic haptic feedback. To reach this, resulting forces during needle insertions (trans- and extrapedicular) into formalin-fixed vertebral specimens were measured. The same insertion procedure was also performed on six customized polyurethane blocks with varying mechanical parameters. Based on the results of these measurements, a specific foam phantom was generated and the insertion force measured. Additionally a parametric model for the needle insertion into bone was designed calculating three characteristic parameters for all insertion measurements. The resulting insertion force for the foam phantom was comparable to the specimen measurements and the parametric model provided comprehensible characteristic parameters. Based on the resulting force during needle insertion into human vertebrae, a possible foam recipe for manufacturing artificial segments was found. Furthermore, the parametric model provides characteristic parameters for the assessment of phantoms as well as the development of its production process.**

***Index Terms*—Artificial vertebrae, kyphoplasty, polyurethane foam**

I. INTRODUCTION

A. Kyphoplasty/Vertebroplasty

Kyphoplasty and vertebroplasty are common treatment opportunities for vertebral compression fractures (VCF's) resulting from osteoporosis and vertebral body tumors. The incidents of VCF's are 700.000 in the USA [1] and 1.4 million in Europe [2]. The thoracolumbar region is mostly affected [3]. In both surgical procedures bone cement (PMMA - polymethylmethacrylate) is injected into the affected vertebra(e), using fluoroscopy for monitoring. The difference between them is that during kyphoplasty the vertebral body is raised by an inflatable balloon before cement injection. A detailed description of kyphoplasty can be found in [4]. Currently the training of these interventions is performed in two different ways. The traditional way of learning skills, following "see one, do one, teach one" is directly performed on patients which affects patient safety and requires a mentor for teaching. The second possibility is to exercise on specimens. Although the anatomical structure is most natural in this case, the costs and especially the availability are limiting factors [5], [6]. Furthermore the usage of a C-arm for fluoroscopic guidance leads to an increased radiation exposure and limits the duration of the surgical training. To manage such problems, an Augmented Reality simulator is going to be developed. Novice surgeons should be able to train the procedure of kyphoplasty or vertebroplasty without radiation exposure and the necessity of specimens. Patient specificity can be integrated through the usage of artificial vertebral phantoms originating from segmented CT-scans and manufactured by appropriate rapid prototyping procedures. The mechanical properties should be comparable to human vertebrae providing realistic haptic feedback.

B. Biomechanical parameters of human vertebrae

Vertebral bodies simply consist of a cortical shell and internal cancellous bone tissue. The thickness of the shell (anterior/posterior and cranial/caudal endplates) is not constant as studies showed [7], [8]. The mean cortical bone mineral densities (BMD) thereby were $413mg/cm^3$ (cranial) and $332mg/cm^3$ (caudal) respectively. A summary of material Young's moduli (E) reported a broad range (0.1 - $12GPa$) mostly tested with finite element methods [9]. On the structural level, trabecular bone segments like cubes or cylinders were mechanically stressed and the structural elastic moduli (stiffness K) were observed for all three loading directions to evidence anisotropy [10], [11]. The mean trabecular BMD decreased from cranial, over thoracic to lumbar vertebrae and resulted in an overall average of $224.8mg/cm^3$ [12]. A lot of studies already dealed with needle insertions into soft tissue [13]. They focused on insertion force modeling, needle steering/deflection and/or motion planning [14], [15]. With reference to kyphoplasty and vertebroplasty, only a few studies exist about force measurements during needle insertion into vertebrae. In [11] a 11 gauge needle was inserted directly into two vertebral bodies (one uncompressed L2, one compressed L3 - imitating a vertebral compression fracture) at three different locations and the resulting insertion force - depth curves were measured. The mean maximum insertion force for L2 was $55N$ at a mean depth of $5.8mm$. Such data could not be identified for L3 due to different trends and no distinctive peaks of the single graphs. In contrast, a 10 gauge needle was used in [16] for a robotic insertion through the pedicles, whereas the results of four different conditions with changing feed rates and rotation speeds were compared. All maximal insertion forces were under $25N$, appearing at a mean depth of $13.11mm$ $(n = 23)$.

[1]Department of Medical Device Engineering, Upper Austria University of Applied Sciences, School of Applied Health and Social Sciences, Garnisonstraße 21, 4020 Linz, Austria.

[2]Department of Biomechanics, Berufsgenossenschaftliche Unfallklinik, Professor Küntscher Straße 8, 82418 Murnau, Germany.

[3]Paracelsus Medical University, Strubergasse 21, 5020 Salzburg, Austria.

978-1-4577-1787-1/12/$26.00 ©2012 IEEE

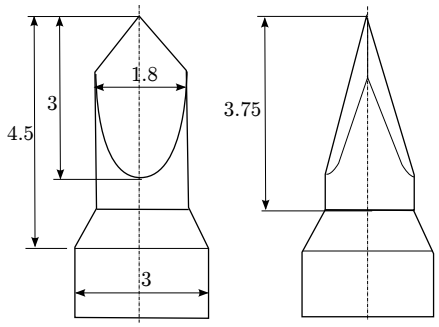

Figure 1: Tool tip geometry, dimensions in mm.

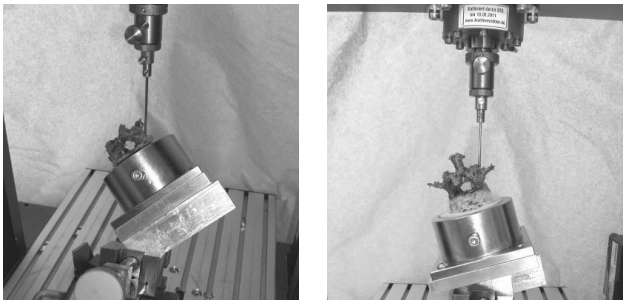

(a) Extrapedicular access (b) Transpedicular access

Figure 2: Specimen test setup

II. MATERIALS AND METHODS

Due to the importance of haptic feedback during bone access, the insertion force was identified as the main validation parameter for the phantom development. Insertion force measurements on specimens were performed to work out the characteristics of force against insertion depth. To test comparability of artificial bone material, tests on customized blocks manufactured with a two-layered structure of different polyurethane (PU) foams were carried out. With the results of these measurements a specific foam phantom was developed and a parametric model designed.

A. Insertion measurement test setting

For all insertion tests, we used the same bone access tool (Kyphon Inc., KyphX Osteo Introducer (11 gauge), Sunnyvale, CA) whose tip geometry is illustrated in Fig. 1. The cannula and its inner needle were separated from the grip to allow a fixation in a special adapter. This adapter was connected to a $2kN$ load cell which in turn was mounted on the horizontal unit of Zwick's Allround Line material testing machine (Zwick GmbH & Co. Kg, Zwick/Roell Z010, Ulm, Germany). The feed rate was $1mm/s$ and the insertion depth varied between 25 and $30mm$ (depending on the access type and the size of the vertebrae). In case of the specimen measurements, the vertebral segments were still surrounded with soft tissue. Therefore an initial force threshold of 5N was specified.

B. Two-layered blocks

Six custom specific blocks (Sawbones Europe AB, Malmö, Sweden) with varying parameters were measured. Each block was manufactured as a two-layered structure imitating the cancellous and cortical build-up of human bone. While only the thickness of the laminate (solid rigid PU foam, density $480mg/cm^3$, compressive strength $18MPa$) changed between 1 and $1.5mm$, three different spongy materials (cellular rigid PU foam, open-cell) with varying density (160, 200 and $320mg/cm^3$ respectively) and compressive strength (2.3, 3.9 and $5.4MPa$ respectively) were used. Finally, the laminated blocks had a dimension of $50 \times 50 \times 41$ and $41.5mm$ respectively. To obtain the homogeneity of the blocks, four insertions on each block were performed.

C. Specimens

Four frozen and formalin fixed thoracolumbar spines of elderly persons were defrosted and their vertebrae (T10 - L2) dissected. Segments with incomplete vertebral arches, transverse or spinous processes as well as segments with distinctive osteophytes were excluded. The remaining 11 segments - 6 for transpedicular and 5 for extrapedicular access (all bilateral) - were embedded in Technovit 3040 (Heraeus Kulzer GmbH, Technovit 3040, Wehrheim, Germany) for fixation and the resulting blocks were clamped in a precision vice. Fig. 2 shows the specimen specific test setup.

D. Foam phantom

According to the results of the specimen and block measurements, a first PU recipe was mixed in collaboration with Hexcel (Hexcel Holding GmbH, Pasching, Austria). The mixture was cast into a simple mold for an easier fixation during the following needle insertion tests. After curing, one side of the block was covered with a resin to imitate the cortical layer. To cast artificial vertebral phantoms, stereolithography models (STL) of T10 and L2 vertebrae were extracted using the DataManager software (BioComputing Competence Center, DataManager, Bologna, Italy). To improve the surface quality they were further processed with the Visualization Toolkit (VTK) library (Kitware Inc., Visualization Toolkit, New York, USA). Using these data sets, primary stereolithography models were generated. Afterwards, two-piece silicone molds were manufactured which were later on used to cast artificial segments.

E. Parametric model for needle insertion

A mathematical model for the needle insertion force provides characteristic parameters for the assessment of phantoms as well as for the development of their production process. The needle insertion force $F_{\text{needle}}(x)$ depends on the insertion depth x and is according to the structure of bone tissue divided into two main parts

$$F_{\text{needle}}(x) = F_{\text{cortical}}(x) + F_{\text{cancellous}}(x).$$

The force F_{cortical} is due to the initial puncture of the vertebra through the stronger cortical bone and $F_{\text{cancellous}}$ reflects the force for penetrating cancellous bone. According to [17] needle forces are attributed to internal stiffness, cutting forces

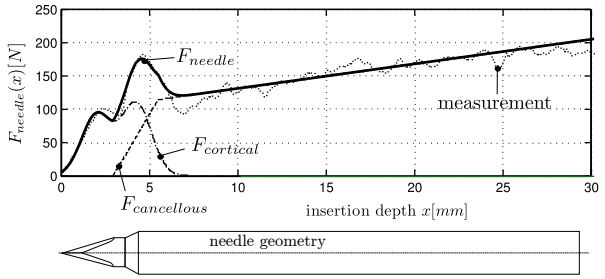

Figure 3: Needle insertion force: model vs. measurement.

and friction. F_{cortical} appears only for the very first part of the insertion process and is dominated by stiffness forces. In contrast, $F_{\text{cancellous}}$ mainly reflects cutting and friction forces. Figure 3 depicts a typical force-displacement graph, which starts with two distinctive peaks caused by elastic forces during needle insertion. The peak location is defined by the varying diameter given by the tool-tip geometry. The remaining part of the graph reflects fluctuating elastic and cutting forces as well as friction forces of the cancellous bone. In [17], the stiffness force was modeled using a second-order polynomial. Due to the tool-tip geometry, the complex situation of cortical bone penetration represented by the force F_{cortical} is modeled by two radial basis functions

$$F_{\text{cortical}}(x) = \sum_{i=1}^{2} w_i e^{-\left(\frac{x-x_{ci}}{\sigma}\right)^2},$$

with common spread $\sigma = 1.2$ and fixed centers at $x_{c1} = 2mm$ and $x_{c2} = 4.25mm$ respectively. The weights w_i are computed out of the measurement data, where the mean value of both weights is used as the first characteristic model parameter. For modeling $F_{\text{cancellous}}$, a mean-value model is used considering the cutting and friction force as

$$F_{\text{cancellous}}(x) = \left(F_{\text{cut}} + f_{\text{friction}}(x - x_0)\right) h_s(x - x_0)$$

and averaging the stiffness force, where both F_{cut} and f_{friction} are used as additional characteristic parameters. Cutting and friction force are fully active, when the needle-tip completely penetrates through the cortical bone which is considered by the Heaviside function $h_s(x - x_0)$ whereas x_0 is defined by the tool-tip geometry. A linear transient region allows a smooth behavior of the cutting force.

III. RESULTS

During all insertion measurements, two interesting sections could be identified. The first one was the penetration of the tool tip (needle and cannula) through the compact layer which happened during the first $6-8mm$ (section 1). Afterwards a section of a nearly constant increase in force followed until the maximum insertion depth was reached (section 2).

A. Two-layered blocks

In Fig. 4 the results for the PU blocks with $1mm$ laminate thickness are illustrated. Because of four insertion measurements on each of the six blocks, only the average curves for the different density values are plotted. The two distinctive

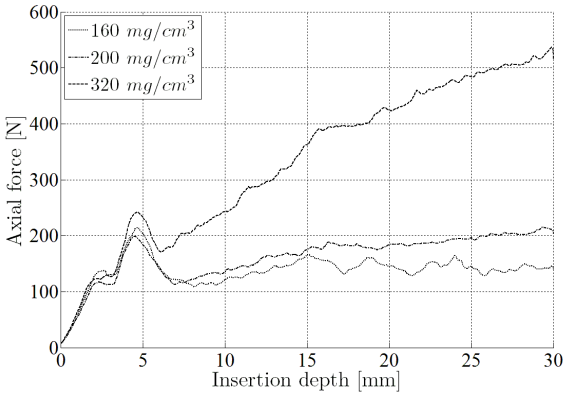

Figure 4: Results for $1mm$ laminate thickness

peaks caused by the tool tip geometry were also visible here. Their maximum values were however different and varied slightly. A reason therefore could be an inhomogeneous filling of underlying pores with laminate material. For the blocks with $1mm$ laminate thickness, the average values of the force peaks ranged from $117N$ to $137.6N$ (peak 1) respectively $198.5N$ to $242.3N$ (peak 2). In case of blocks with $1.5mm$ laminate thickness they ranged from $130.6N$ to $191.5N$ respectively $223.1N$ to $250.7N$. Concerning the varying density values of the cancellous material, the resulting force progressions showed different slopes in section 2. With increasing density values, the friction surface between the insertion tool and the cancellous material became greater and the forces rose stronger.

B. Specimens

The average force progression with corresponding standard deviation (SD) for transpedicular access is shown in Fig. 5 whereas the specimen average is drawn as a bold line. A wide spread between the particular measurements has been observed due to the fact that biomechanical parameters, like density or bone strength, vary between individual vertebral segments. At transpedicular access, the average force curve showed two distinctive peaks in section 1 where the influence of the tool tip geometry became visible. The first peak occurred after the inner needle tip penetrated fully through the compact structure. This was followed by a slight decrease of the needle force which represented a short segment of constant cross-section (see Fig. 1). The second one was characteristic for the sharpened geometry of the cannula, which also had to penetrate through the compact structure. The maximum force values of the peaks were $52.2N$ respectively $73.8N$. Because of a thinner cortical layer at the lateral vertebral wall, the force peaks were not so clearly visible at extrapedicular access. Compared to the results of the block measurements, the characteristics of the specimen measurements were almost the same. The insertion forces of the block measurements in general were considerably while the increase in force during section 2 was in the range of the block measurements. To imitate those specimens a density value of 160 - $200mg/cm^3$ would be appropriate.

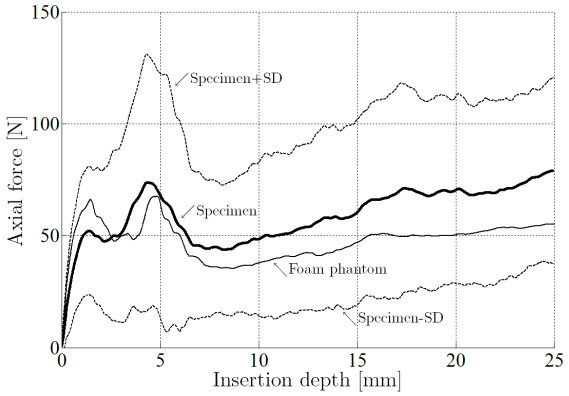

Figure 5: Resulting average curves

C. Foam phantom

The resulting average curve of the foam phantom is depicted in Fig. 5 and is clearly within the standard deviation of the specimen measurement. Also the characteristics concerning the two distinctive peaks or the increase of force in section 2 are comparable.

D. Parametric model for needle insertion

The results of the parametric model are summarized in Fig. 6. The characteristic parameters F_{cut}, f_{friction} and $mean(w_i)$ were obtained by fitting the model to the measurement data using a Gauss-Newton method and are illustrated in Fig. 6 for the Sawbones blocks (density values respectively laminate thickness), the transpedicular specimen measurement (spine tp) and the foam phantom (foam). Concerning the friction force f_{friction}, the model calculated increasing values with rising density for the Sawbones block measurements which is consistent to the results illustrated in Fig. 4. The friction forces of the specimen and foam phantom measurements calculated were comparable having less spread. Together with the fact that also their cutting forces F_{cut} were in the same range, respectively higher for the specimens, these findings agree with Fig. 5 indicating a lower average curve for the foam phantom in section 2. As expected, the largest spreads for the cutting force as well as the weights were calculated for the specimen measurements.

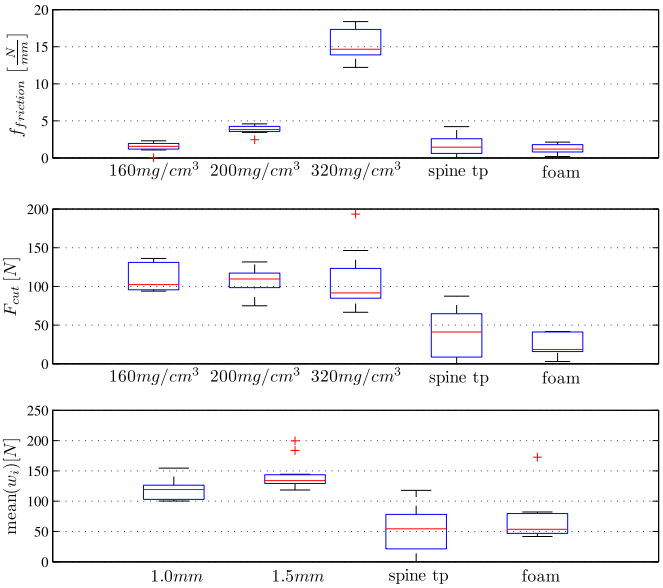

Figure 6: Characteristic parameters

ACKNOWLEDGMENTS

The authors would like to express their thanks to Vithaldas Guru (Hexcel Pasching, Austria) for excellent assistance in developing a potential foam recipe.

REFERENCES

[1] L. J. Melton, M. Thamer, N. F. Ray, J. K. Chan, C. H. Chesnut, T. A. Einhorn, C. C. Johnston, L. G. Raisz, S. L. Silverman, and E. S. Siris. Fractures attributable to osteoporosis: report from the national osteoporosis foundation. *J Bone Miner Res*, 12(1):16–23, Jan 1997.

[2] Incidence of vertebral fracture in europe: results from the european prospective osteoporosis study (epos). *J Bone Miner Res*, 17(4):716–724, Apr 2002.

[3] R. D. Wasnich. Vertebral fracture epidemiology. *Bone*, 18(3 Suppl):179S–183S, Mar 1996.

[4] Pierre Hardouin, Paul Fayada, Hervé Leclet, and Daniel Chopin. Kyphoplasty. *Joint Bone Spine*, 69(3):256–261, May 2002.

[5] Arne Radetzky and Andreas Nürnberger. Visualization and simulation techniques for surgical simulators using actual patient's data. *Artif Intell Med*, 26(3):255–279, Nov 2002.

[6] Shawn Tsuda, Daniel Scott, Jennifer Doyle, and Daniel B Jones. Surgical skills training and simulation. *Curr Probl Surg*, 46(4):271–370, Apr 2009.

[7] Nicola L Fazzalari, Ian H Parkinson, Quentin A Fogg, and Peter Sutton-Smith. Antero-postero differences in cortical thickness and cortical porosity of t12 to l5 vertebral bodies. *Joint Bone Spine*, 73(3):293–297, May 2006.

[8] Yue Wang, Michele C Battié, Steven K Boyd, and Tapio Videman. The osseous endplates in lumbar vertebrae: thickness, bone mineral density and their associations with age and disk degeneration. *Bone*, 48(4):804–809, Apr 2011.

[9] H. S. Kim and S. T S Al-Hassani. A morphological model of vertebral trabecular bone. *J Biomech*, 35(8):1101–1114, Aug 2002.

[10] P.H.F. Nicholson, X.G. Cheng, G. Lowet, S. Boonen, M.W.J. Davie, J. Dequeker, and G. Van der Perre. Structural and material mechanical properties of human vertebral cancellous bone. *Medical Engineering & Physics*, 19(8):729 – 737, 1997.

[11] S. H. Teoh and C. K. Chui. Bone material properties and fracture analysis: needle insertion for spinal surgery. *J Mech Behav Biomed Mater*, 1(2):115–139, Apr 2008.

[12] Narayan Yoganandan, Frank A Pintar, Brian D Stemper, Jamie L Baisden, Recyi Aktay, Barry S Shender, Glenn Paskoff, and Purushottam Laud. Trabecular bone density of male human cervical and lumbar vertebrae. *Bone*, 39(2):336–344, Aug 2006.

[13] Niki Abolhassani, Rajni Patel, and Mehrdad Moallem. Needle insertion into soft tissue: a survey. *Med Eng Phys*, 29(4):413–431, May 2007.

[14] N. Chentanez, R. Alterovitz, D. Ritchie, L. Cho, K. K. Hauser, K. Goldberg, J. R. Shewchuk, and J. F. O'Brien. Interactive simulation of surgical needle insertion and steering. *ACM SIGGRAPH conference proceedings*, 2009.

[15] Simon P. DiMaio and S. E. Salcudean. Needle steering and motion planning in soft tissues. *IEEE Trans Biomed Eng*, 52(6):965–974, Jun 2005.

[16] Kiyoshi Matsumiya, Yasuyuki Momoi, Etsuko Kobayashi, Nobuhiko Sugano, Kazuo Yonenobu, Hiroshi Inada, Takayuki Tsuji, and Ichiro Sakuma. Forces and torques during robotic needle insertion to human vertebra. *International Congress Series*, 1256:492 – 497, 2003. CARS 2003. Computer Assisted Radiology and Surgery. Proceedings of the 17th International Congress and Exhibition.

[17] A.M. Okamura, C. Simone, and M.D. O'Leary. Force modeling for needle insertion into soft tissue. *Biomedical Engineering, IEEE Transactions on*, 51(10):1707 –1716, oct. 2004.